PHOTONICS Research

Mid-infrared photon counting and resolving via efficient frequency upconversion

Kun Huang,[1,*] Yinqi Wang,[1] Jianan Fang,[1] Weiyan Kang,[2] Ying Sun,[2] Yan Liang,[2] Qiang Hao,[2] Ming Yan,[1] and Heping Zeng[1,3,4,5,6]

[1]State Key Laboratory of Precision Spectroscopy, East China Normal University, Shanghai 200062, China
[2]School of Optical Electrical and Computer Engineering, University of Shanghai for Science and Technology, Shanghai 200093, China
[3]Jinan Institute of Quantum Technology, Jinan 250101, China
[4]CAS Center for Excellence in Ultra-intense Laser Science, Shanghai 201800, China
[5]Shanghai Research Center for Quantum Sciences, Shanghai 201315, China
[6]e-mail: hpzeng@phy.ecnu.edu.cn
*Corresponding author: khuang@lps.ecnu.edu.cn

Received 18 September 2020; revised 23 December 2020; accepted 27 December 2020; posted 5 January 2021 (Doc. ID 410302); published 1 February 2021

Optical detectors with single-photon sensitivity and large dynamic range would facilitate a variety of applications. Specifically, the capability of extending operation wavelengths into the mid-infrared region is highly attractive. Here we implement a mid-infrared frequency upconversion detector for counting and resolving photons at 3 μm. Thanks to the spectrotemporal engineering of the involved optical fields, the mid-infrared photons could be spectrally translated into the visible band with a conversion efficiency of 80%. In combination with a silicon avalanche photodiode, we obtained unprecedented performance with a high overall detection efficiency of 37% and a low noise equivalent power of 1.8×10^{-17} W/Hz$^{1/2}$. Furthermore, photon-number-resolving detection at mid-infrared wavelengths was demonstrated, for the first time to our knowledge, with a multipixel photon counter. The implemented upconversion detector exhibited a maximal resolving photon number up to 9 with a noise probability per pulse of 0.14% at the peak detection efficiency. The achieved photon counting and resolving performance might open up new possibilities in trace molecule spectroscopy, sensitive biochemical sensing, and free-space communications, among others.

https://doi.org/10.1364/PRJ.410302

1. INTRODUCTION

The mid-infrared (MIR) wavelength region is of great interest for a variety of applications as wide-ranging as environmental monitoring, molecular spectroscopy, biomedical sensing, and free-space communication [1,2]. In these envisioned scenarios, sensitive MIR detection is highly demanded to access dramatically improved performance in terms of detection sensitivity, working distance, or imaging functionality [3]. So far, tremendous progress has been witnessed in developing MIR detectors based on either conventional semiconductors of indium antimonide (InSb) and mercury cadmium telluride (MCT), or emerging materials of colloidal quantum dots [4], graphene plasmons [5], and black phosphorus [6]. However, the noise-equivalent power (NEP) is typically limited to about pW/Hz$^{1/2}$, far below the level of single-photon detection. The attainable sensitivity could be improved with cryogenic operation for suppressing the intrinsic blackbody radiation and dark current. Notably, MIR single-photon detection has been accessed by superconducting nanowire detectors [7], albeit with additional complexity of a bulky cooling system. Very recently, a broadband response window from 1.55 to 5.07 μm was achieved with an optimized width of MoSi-based nanowire [8]. Nowadays, continuous endeavors have still been dedicated to approaching efficient direct detection for MIR photons, especially at room temperature.

Indeed, the performance of currently existing MIR detectors is in marked contrast to the visible and near-infrared regions, in which highly efficient and low-noise photon counting is available by commercial avalanche photodiodes (APDs) [9]. Especially, photon-number-resolving (PNR) capability has also been readily achieved using a silicon-based multipixel photon counter (Si-MPPC). The resulting single-photon sensitivity and large dynamic range could not only support accurate and rapid characterization of nonrepetitive optical signal at low-light levels, but also facilitate quantum-optics experiments to investigate multiphoton quantum states [10,11], measure high-order correlation functions [12], and characterize Wigner functions [13]. Moreover, photon-number identification also constitutes a key enabler in promising protocols in quantum information science, such as thresholded laser ranging [14],

loss-tolerant optical communication [15], and high-capacity or long-distance quantum key distribution [16,17].

In view of the attractive features of Si-based detectors, frequency upconversion strategy by spectrally translating the MIR signals into shorter wavelengths has been recognized as a simple yet effective way to capture MIR photons. Recently, such an indirect MIR approach has been investigated by utilizing optical nonlinearities based on crystals [18–21], waveguides [22,23], nanowires [24], as well as fluorophore [25]. A similar spirit was also manifested in MIR detection based on nondegenerate two-photon absorption in wide-bandgap semiconductors [26]. Current advances in frequency upconversion detectors have even led to demonstrating sensitive MIR imaging by high-definition Si-based CCD cameras [27,28], with great potential to extend the working wavelength into the far-infrared regime [29]. However, to date, the conversion efficiency achieved for MIR single-photon upconverters is typically below 35% [19,21,27]. These limited values contrast with the near-infrared counterparts with nearly complete conversion [30–33]. Moreover, stringent filtering stages are typically needed to suppress the severe pump-induced parametric fluorescence noise, which ultimately results in an MIR detection efficiency of several percentage points [34]. Consequently, PNR detection at MIR has not yet been reported due to the limited efficiency and accompanying background noise, although the desirable feature was demonstrated a decade ago at 1.56 μm [35] and 1.04 μm [36]. Nowadays, there is a significant impulse to move quantum optics to the MIR [20,37,38], thus urgently calling for enabling techniques to yield efficient single-photon counting and photon-number resolution.

Here we demonstrate a high-performance MIR frequency upconversion detector based on the coincidence pumping configuration. Thanks to the spectrotemporal optimization for the passively synchronized pulses, the intrinsic conversion efficiency for the MIR photons at 3 μm reached 80%. Correspondingly, the overall detection efficiency of about 37% could be achieved due to the effective filtering system. The resultant noise equivalent power (NEP) was as low as 1.8×10^{-17} $\mathrm{W/Hz^{1/2}}$, thus representing the highest sensitivity among reported MIR detectors. Furthermore, we demonstrated for the first time, to the best of our knowledge, the ability to resolve the number of photons within an MIR pulse. The obtained MIR photon counting and resolving performances would pave the way toward implementing advanced protocols, which require an ultimate sensitivity at the single-photon level and a large dynamic range with linear response to incident photon numbers.

2. PRINCIPLE OF COHERENT FREQUENCY CONVERSION

Coherent frequency upconverters enable the translation of the frequency of signal photons into a higher targeted one while preserving the optical coherences or quantum characteristics [39]. The involved nonlinear process is usually realized by the second-order sum-frequency generation (SFG) under the nondepleted pump approximation. The energy conservation leads to $\omega_1 + \omega_2 = \omega_3$, where 1, 2, 3 denote the signal, pump, and SFG modes, respectively. Under the perfectly phase-matching condition, the relevant Hamiltonian for the three-wave mixing is given as

$$\hat{H} = i\hbar g\alpha(\hat{a}_1\hat{a}_3^{\dagger} - \text{H.c.}), \tag{1}$$

where α is the electric amplitude of the classical pump field, g is the coupling constant determined by the nonlinear susceptibility of the medium, and H.c. represents the Hermitian conjugate. $\hat{a}_1$ and $\hat{a}_3$ denote the annihilation operators for the signal and converted photons, respectively. Using this Hamiltonian, the state evolution after an interaction length L can be described by the coupled-mode equations as

$$\hat{a}_3(L) = \sin(|g\alpha|L)\hat{a}_1(0) + \cos(|g\alpha|L)\hat{a}_3(0). \tag{2}$$

A complete conversion, $\hat{a}_3(L) = \hat{a}_1(0)$, can be obtained if $|g\alpha|L = \pi/2$. In this case, the signal photon is annihilated at the creation of the SFG photon. The one-to-one correspondence ensures a noiseless conversion, which forms the basis for many applications such as single-photon detection and optical quantum interface [39]. Generally, the conversion efficiency can be defined by

$$\begin{aligned}\eta &= N_3(L)/N_1(0) = \eta_m \sin^2(|g\alpha|L) \\ &= \eta_m \sin^2(\pi/2\sqrt{P/P_m}),\end{aligned} \tag{3}$$

where $N_i = \langle\hat{a}_i^{\dagger}\hat{a}_i\rangle$ denotes the average photon number, P is the pump power, and η_m is the maximum conversion efficiency under a pump power of P_m.

Similarly, the inverse process acting as a coherent downconverter (CDC) is possible by noticing the Hermitian conjugated term in Eq. (1). In this scenario, the signal photon with the higher frequency ω_3 could be completely converted to a photon with a lower frequency ω_1 [40]. Therefore, an identical solution for the quantum state evolution could be expected, and the conversion efficiency shows the same dependence on the pump power as given by Eq. (3). A CDC was used in our experiment to prepare the MIR signal from the near-infrared coherent light. Specifically, the linear response of the downconverter provides a solution for precisely calibrating the MIR power, especially at the single-photon level. Indeed, measuring MIR light at low powers is typically challenging due to limited power-meter sensitivity and ambient thermal disturbance. To this end, well-calibrated attenuators were inserted in the near-infrared light path, which could result in the same attenuation for the MIR output. In the following, we will turn to the experimental realization of the aforementioned coherent converters.

3. EXPERIMENTAL SETUP

As discussed above, two complementary nonlinear optical processes, i.e., coherent frequency down- and upconversion, were used in our experiment. Figure 1(a) illustrates the related energy transition diagram based on three-wave mixing. Specifically, the CDC enables the preparation of the MIR source from a weak near-infrared light at 1030 nm under pumping at 1550 nm. In principle, the MIR signal would preserve quantum and coherent properties of the near-infrared states [41], which thus provides an effective way to prepare quantum states at MIR, such as squeezed states and entangled states. The prepared MIR source here should be in a coherent

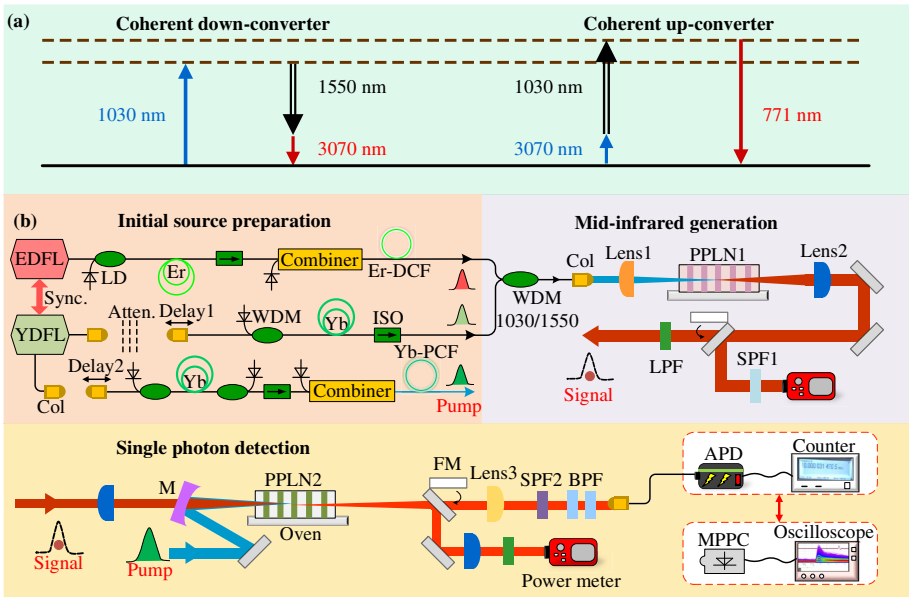

Fig. 1. (a) Energy transition diagram for coherent down- and upconverters based on a second-order nonlinear process. The downconverter is used to prepare an MIR source with a well-calibrated power, which is essential in characterizing the detection performances for the MIR upconverter. (b) Experimental setup for MIR upconversion detection system based on passively synchronized fiber lasers. Initial source preparation for subsequent nonlinear conversion was realized by two Er- and Yb-doped fiber lasers (EDFL and YDFL) and multistage fiber amplifiers. The resultant amplified pulses at 1.03 and 1.55 μm were used to generate the MIR signal. Another branch of amplified pulse at 1.03 μm served as the pump, which was used to spectrally convert the MIR signal to the visible band for efficient single-photon and PNR detection. LD, laser diode; WDM, wavelength division multiplexer; Col, collimator; ISO, isolator; Yb/Er, ytterbium- or erbium-doped gain fiber; DCF, double-clad fiber; PCF, photonic crystal fiber; Atten, neutral density attenuator; M, dichroic concave mirror; FM, flip mirror; PPLN, periodically poled lithium niobate crystal; SPF, LPF, and BPF: short-, long-, and bandpass filter; APD, avalanche photodiode; MPPC, multipixel photon counter.

state, which will be verified later by the photon-number distribution measured by a PNR detector. Another desirable feature for the CDC was the possibility of calibrating the MIR power, particularly at the single-photon level by adding attenuators for the near-infrared light. Indeed, the attenuation for near-infrared wavelengths could be better calibrated due to more sensitive optical detectors. As for the coherent upconverter (CUD), it can spectrally translate the MIR signal into the visible band under pumping at 1030 nm, which enables MIR single-photon counting and PNR detection.

The experimental realization is presented in Fig. 1(b), including the three parts of the initial source preparation, MIR signal generation, and single-photon detection. All the light sources originated from a passively synchronized fiber laser system, which consisted of two Er- and Yb-doped fiber lasers (EDFL and YDFL). The two fiber lasers were arranged in a shared-cavity configuration. Cross-phase modulation between the dual-color pulses within a common section of single-mode fiber could result in synchronous mode-locking at 14.6 MHz. More details about the all-optical synchronization may be found in Ref. [42]. The YDFL output at 1029.8 nm was divided into two portions, which served as the seed and pump for the CDC and CUC modules, respectively. The power of the pump could be amplified to the watt level based on photonic crystal gain fiber. Thanks to the large mode diameter, a narrow spectrum was maintained during the amplification, resulting in a 0.12-nm full width at half-maximum (FWHM), as shown in Fig. 2(a). The corresponding pulse duration was inferred to be

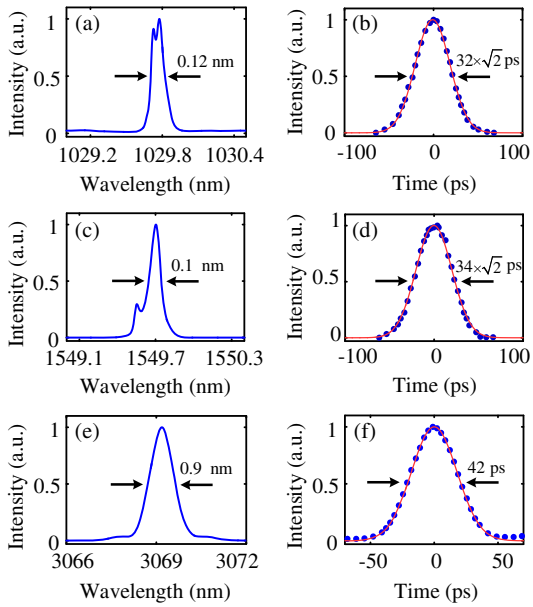

Fig. 2. Spectrotemporal characterization of involved light pulses. (a) and (c) are the measured optical spectra for the output pulses from the YDFL and EDFL, respectively. (b) and (d) give the corresponding autocorrelation traces. A scaling factor of $\sqrt{2}$ was taken to deduce the actual pulse duration with the assumption of a Gaussian profile. (e) Optical spectrum for the MIR signal source; (f) cross-correlation trace between signal and pump pulses.

32 ps from the measured autocorrelation trace in Fig. 2(b). Note that a scaling factor of $\sqrt{2}$ was used under the assumption of a Gaussian profile. Similarly, the power of the EDFL output was boosted to about 200 mW by using cascaded fiber amplifiers. The corresponding optical spectrum is shown in Fig. 2(c), which indicated a center wavelength at 1549.7 nm and an FWHM of 0.1 nm. The inferred pulse duration was 34 ps, as given in Fig. 2(d).

The dual-color pulses at 1 and 1.55 μm were then spatially combined with a wavelength division multiplexer (WDM). The mixed light was collimated into the free space before being focused into a periodically poled lithium niobate (PPLN) crystal. A quasi-phase-matching condition was optimized at an operation temperature of 40.7°C and a polling period of 30.3 μm, leading to efficient generation of MIR light at 3069 nm. The resultant narrow spectral bandwidth of 0.9 nm, as shown in Fig. 2(e), would favor efficient nonlinear conversion within the phase-matching window. To generate the MIR signal, the pump power at 1.55 μm was arbitrarily set around 120 mW, corresponding to a downconversion efficiency of 40%. The linear relationship between the powers at 1 and 3 μm was verified by inserting calibrated neutral density filters (NDFs) within the delay line (Delay1). Therefore, the MIR power could be precisely controlled by choosing a proper combination of NDFs at the near-infrared. The attenuated MIR light will serve as the signal source for the subsequent CUC module.

To implement the frequency upconversion detector, the signal and pump sources were spatially combined by a dichroic concave mirror and temporally overlapped with a translational stage (Delay2). Another PPLN crystal was used to perform the SFG, which has a length of 25 mm. The resultant phase-matching window for the nonlinear crystal was about 5 nm in the case of narrowband pumping [27], which was much larger than the spectral bandwidth of the MIR signal. As shown in the inset of Fig. 3, the phase-matching temperature was about 54.6°C for the chosen poling period of 20.9 μm. The resulting SFG signal at 771 nm was then sent into filtering stages before being registered by Si-based detectors. Based on SFG configuration, a cross-correlation trace was measured with an FWHM of 42 ps, as shown in Fig. 2(f). In the weak conversion regime, the cross-correlation bandwidth depends on the convolution between the signal and pump pulses, which indicated a pulse duration of 27 ps for the MIR signal. In this case, the MIR photons would be temporally confined within the pump envelope, thus ensuring a high total conversion efficiency [32].

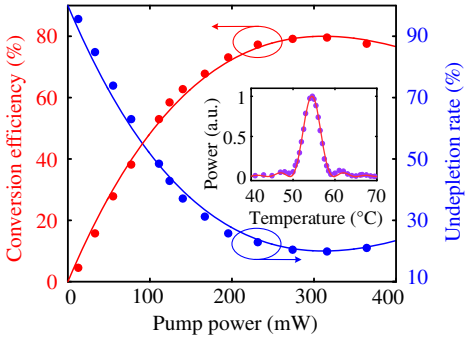

Fig. 3. Conversion efficiency and undepletion rate as functions of the pump power. The MIR signal was set at the megawatt level, thus ensuring the fulfillment of the nondepleted pump approximation. The solid lines are given by the theoretical model in the text. The inset shows the phase-matching behavior depending on the crystal temperature.

4. RESULTS AND DISCUSSIONS

Now we turn to characterize the performance of the implemented upconversion detector. Conversion efficiency is a crucial parameter that defines the possibility for an MIR photon to be converted. Practically, the conversion efficiency η could be measured by evaluating the power ratio between the signal and upconverted light as $\eta = (P_{\mathrm{up}}/P_s) \times (\lambda_{\mathrm{up}}/\lambda_s)$. Figure 3 shows the deduced conversion efficiency as varying the pump power, which was fitted by Eq. (3) with $\eta_m = 80\%$ and $P_m = 312$ mW. As expected, excessive pumping power resulted in the decrease of the conversion efficiency due to the complementary downconversion process [30]. To further validate the achieved efficiency, we also measured the so-called undepletion rate $R = 1 - \eta = P_{\mathrm{res}}/P_0$, where P_0 and P_{res} are the input and residual MIR signal power, respectively. The advantages of the proposed method lie in the avoidance to calibrate power measurement devices for different wavelengths, and the independence from losses including propagation transmission and filtering efficiency. The measured undepletion rate shown in Fig. 3 was modeled quite well with the previously obtained parameters. The high conversion efficiency was due to the careful optimization of optical pulses in spectral and temporal domains [43]. First, the spectrum of the MIR signal was made to be narrow for approaching the efficient phase-matching window. Second, the pulse duration of the MIR signal was set to be smaller than that of the pump, which ensured a sufficiently intensive pump field for signal photons. Third, the relative timing jitter of the synchronized signal and pump pulses was negligible relative to the pulse duration, thus permitting a stable and efficient nonlinear interaction.

In principle, the unitary conversion efficiency was possible in the case of a perfectly phase-matching condition and sufficient pump intensity [39]. To go beyond the achieved conversion efficiency, we could resort to a better temporal matching of the signal and pump pulses [32]. Rigorously, the total conversion efficiency $\bar{\eta}$ should depend on the pulse overlapping as

$$\bar{\eta} = \frac{\int_{-\infty}^{+\infty} \sin^2[\pi/2\sqrt{I_p(t)/I_p(0)}] \times I_s(t)\mathrm{d}t}{\int_{-\infty}^{+\infty} I_s(t)\mathrm{d}t}, \tag{4}$$

where $I_p(t)$ and $I_s(t)$ denote the intensity profiles for the pump and signal pulses, respectively. In our experiment, the 32-ps pump and 27-ps signal pulses would result in a conversion efficiency of about 90%. Another limiting factor might be ascribed to the spatial-mode mismatching for the focused pump and signal beams within the nonlinear crystal.

In the following, we proceed to investigate the photon-counting performance for the MIR upconversion detector. To emulate the single-photon source, the MIR signal was intensively attenuated to contain 0.127 photons per pulse. As discussed above, the attenuation was determined by adding a series of properly calibrated NDFs into the near-infrared light

path. The SFG signal was sent through a short-pass filter with a cutoff wavelength of 900 nm and two bandpass filters with a bandwidth of 10 nm. The total transmission of the filters η_f was about 92%, with a noise rejection of 130 dB at the pump wavelength. The filtered light was then coupled into a single-mode fiber with a coupling efficiency η_c of 87%, which could act as an effective spatial filtering for upconverted parametric fluorescences [44]. The resulting background noise N_b at the peak conversion efficiency was about 5.4 kHz, as shown in the inset of Fig. 4. Finally, the upconverted photons were registered by a fiber-coupled single-photon counting module (SPCM) with a detection efficiency η_{SPCM} of 58% at 771 nm and a dark noise of about 100 Hz. The overall detection efficiency could be evaluated by dividing the recored count rate by the input MIR photon flux of 1.854 MHz. Specifically, the maximum count rate of 687 kHz was recorded at the peak conversion efficiency, which indicated a detection efficiency η_d of 37%, as shown in Fig. 4. After correction for the total loss given by $\eta_f \times \eta_c \times \eta_{\mathrm{SPCM}} = 46\%$, the conversion efficiency for MIR single photons was calculated to be 80%, which was identical to that obtained in the weak signal regime. Furthermore, sensitivity of the upconversion detector was evaluated with the NEP defined by $\mathrm{NEP} = \hbar\omega\sqrt{2N_b}/\eta_d$, where $\hbar\omega$ is the MIR photon energy [30]. As shown in Fig. 4, a low NEP of 1.8×10^{-17} $\mathrm{W/Hz^{1/2}}$ was realized at the maximum detection efficiency. The demonstrated sensitivity down to the single-photon level was at least 4 orders of magnitude better than conventional detectors based on PbS, PbSe, and HgCdTe [34]. Moreover, the NEP for the MIR upconversion detector was more than 10 times lower than that for the state-of-the-art superconducting nanowire single-photon detector with a detection efficiency about 4% at 3 μm and a dark count rate over 10 kHz [7].

In order to demonstrate the PNR capability, the SPCM was replaced by a Si-MPPC. The MPPC (Hamamatsu Photonics S13362-3050DG) comprised 60 × 60 pixels on an effective active area of 9 $\mathrm{mm^2}$. The underlying mechanism for the PNR detection was based on the spatial multiplexing, where incident photons would randomly hit different pixels. The breakdown voltage was optimized at 53 V for approaching a trade-off among quantum efficiency, dark noise, and photon-number resolution. The detection efficiency η_{MPPC} was about 8% at 771 nm, with a dark noise of about 15 kHz. The electronics for readout and processing were optimized for a high repetition-rate operation at 14.6 MHz, which was much higher than previously reported values below several megahertz [35,36]. Figure 5(a) shows the typical waveforms recorded by a digital oscilloscope at the persistence display mode. The sampling rate was set at 20 GHz, which was sufficient to identify the photon clicks within a temporal duration about 4 ns. The exhibiting discrete amplitudes correspond to various detected photon numbers. Figure 5(b) gives the histogram of the voltage amplitude for the acquired 500,000 MPPC waveforms. Different photon-number states could be differentiated by the peaks in the histogram, leading a maximum resolved photon number up to 9. These peaks were then fitted by a series of Gaussian functions. The area under each peak after being normalized to the total one represents the photon-number probability. The reconstructed photon-number distribution is given in Fig. 5(c).

Generally, the measured probability $Q(n)$ for n photons in the pulse is related to the incoming distribution $S(m)$ by the relation: $Q(n) = \sum_{m \geq n} P(n|m) \times S(m)$, where $P(n|m)$ is the conditional probability that n photons are detected at the presence of m incident photons. In our proof-of-principle experiment, the MIR signal was in a coherent state, thus following the Poissonian nature for the photon-number statistics. In this case, the detected state after losses was still a coherent state, but with a smaller average photon number scaled by the overall detection efficiency. As shown in Fig. 5(c), the photon-number distribution was close to a Poissonian $Q(n) = \mu^n \exp(-\mu)/n!$, with a detected average photon number of $\mu = 2.55$. The linear scaling between the detected and input average photon

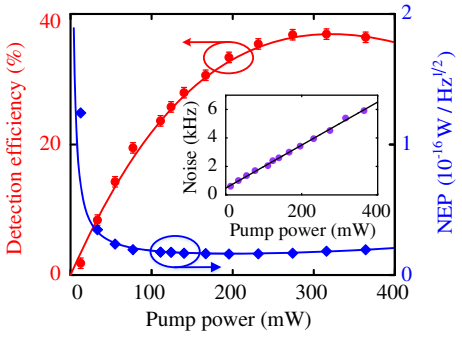

Fig. 4. Detection efficiency and NEP versus the pump power for the implemented frequency upconversion detector. The input MIR signal was set at the single-photon level with an average photon number of 0.13 per pulse. The solid lines are given by the theoretical mode in the text. Count rates for the background noise are given in the inset.

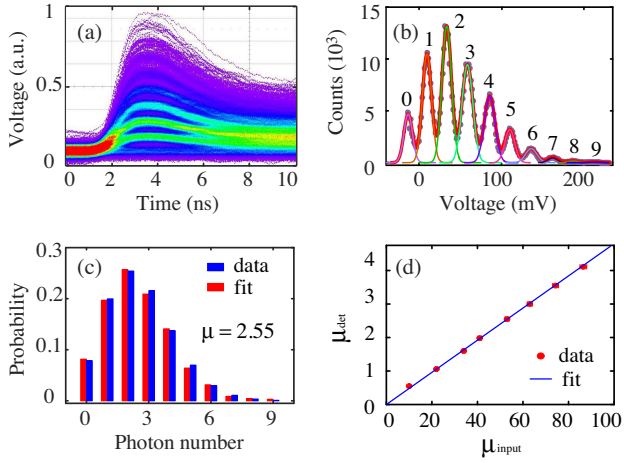

Fig. 5. PNR performance for the MIR frequency upconversion detector based on a Si-MPPC. (a) Superimposed waveforms of the MPPC signal recorded by a digital oscilloscope; (b) histogram of the photoresponse voltage amplitude for the upconverted SFG pulses. The solid lines represent the Gaussian fits, while the numbers denote the corresponding photon-number states. (c) Photon-number distribution reconstructed from the results shown in (b). The obtained statistics are fitted by Poisson distribution, indicating an average photon number of 2.55 per pulse. (d) Detected average photon number as a function of the incident average photon number. The slope of the fitted linear line implies a detection efficiency of 4.8%.

numbers per pulse is manifested in Fig. 5(d), which shows a large dynamic range for the incident MIR power. The slope of the linear fitting line indicates a total detection efficiency of 4.8%, which includes the conversion efficiency, filtering transmission, and detection efficiency of the MPPC. The detection efficiency could be further increased by choosing an MPPC with higher responsivity optimized at the SFG wavelength [36]. Thanks to the low-noise upconversion system and high-speed repetition rate, the achieved noise probability was as low as 1.4×10^{-3}, which would impose negligible effect on the PNR performance. In our experiment, the background noise for the upconversion PNR detector was mainly limited by the dark noise from the detector itself. The intrinsic thermal noise could be minimized by using Peltier cooling [36].

5. SUMMARY

To conclude, we have demonstrated MIR photon counting and resolving performance based on efficient nonlinear frequency upconversion. The employed pulsed pumping scheme leveraged the high peak power and ultrashort excitation window, which helps to increase the conversion efficiency and reduce the background noise. Thanks to the spectrotemporal engineering and tight passive synchronization of the involved light pulses, the quantum conversion efficiency was optimized up to 80%. In combination of effective filtering stage and high-performance Si-SPCM, a record-high overall detection efficiency of 37% was obtained with a corresponding NEP as low as 1.8×10^{-17} W/Hz$^{1/2}$. The presented upconversion detector was thus featured with ultrahigh sensitivity at the room-temperature operation. Furthermore, the upconversion detector was extended with a Si-MPPC to demonstrate a heretofore uninvestigated PNR capability at MIR. The maximum resolved photon number reached 9, which enabled the implementation of a faithful reconstruction of Poissonian statistics for MIR coherent states. The achieved MIR photon recording and resolving capabilities promise to facilitate subsequent classical and quantum applications requiring single-photon sensitivity and large dynamic range, such as high-precision remote positioning [45], ultrasensitive gas sensing [46], photon-number-thresholded lidar [14,47], and quantum communication through a complex scattering channel [48].

Funding. National Key Research and Development Program of China (2018YFB0407100); Science and Technology Innovation Program of Basic Science Foundation of Shanghai (18JC1412000); Program for Professor of Special Appointment (Eastern Scholar) at Shanghai Institutions of Higher Learning; National Natural Science Foundation of China (11621404, 11727812); Shanghai Municipal Science and Technology Major Project (2019SHZDZX01).

Disclosures. The authors declare no conflicts of interest.

REFERENCES

1. M. Ebrahim-Zadeh and I. T. Sorokina, eds., *Mid-Infrared Coherent Sources and Applications* (Springer, 2008).
2. K. L. Vodopyanov, *Laser-Based Mid-Infrared Sources and Applications* (Wiley, 2020).
3. M. Razeghi and B.-M. Nguyen, "Advances in mid-infrared detection and imaging: a key issues review," Rep. Prog. Phys. **77**, 082401 (2014).
4. S. Keuleyan, E. Lhuillier, V. Brajuskovic, and P. Guyot-Sionnest, "Mid-infrared HgTe colloidal quantum dot photodetectors," Nat. Photonics **5**, 489–493 (2011).
5. Q. Guo, R. Yu, C. Li, S. Yuan, B. Deng, F. Javier García de Abajo, and F. Xia, "Efficient electrical detection of mid-infrared graphene plasmons at room temperature," Nat. Mater. **17**, 986–992 (2018).
6. J. Bullock, M. Amani, J. Cho, Y.-Z. Chen, G. H. Ahn, V. Adinolfi, V. R. Shrestha, Y. Gao, K. B. Crozier, Y.-L. Chueh, and A. Javey, "Polarization-resolved black phosphorus/molybdenum disulfide mid-wave infrared photodiodes with high detectivity at room temperature," Nat. Photonics **12**, 601–607 (2018).
7. F. Marsili, F. Bellei, F. Najafi, A. E. Dane, E. A. Dauler, R. J. Molnar, and K. K. Berggren, "Efficient single photon detection from 500 nm to 5 μm wavelength," Nano Lett. **12**, 4799–4804 (2012).
8. Q. Chen, R. Ge, L. Zhang, F. Li, B. Zhang, Y. Dai, Y. Fei, X. Wang, X. Jia, Q. Zhao, X. Tu, L. Kang, J. Chen, and P. Wu, "Mid-infrared single photon detector with superconductor $Mo_{80}Si_{20}$ nanowire," arXiv:2011.06699 (2020).
9. R. H. Hadfield, "Single-photon detectors for optical quantum information applications," Nat. Photonics **3**, 696–705 (2009).
10. T. Gerrits, S. Glancy, T. S. Clement, B. Calkins, A. E. Lita, A. J. Miller, A. L. Migdall, S. W. Nam, R. P. Mirin, and E. Knill, "Generation of optical coherent-state superpositions by number-resolved photon subtraction from the squeezed vacuum," Phys. Rev. A **82**, 031802 (2010).
11. N. Namekata, Y. Takahashi, G. Fujii, D. Fukuda, S. Kurimura, and S. Inoue, "Non-Gaussian operation based on photon subtraction using a photon-number-resolving detector at a telecommunications wavelength," Nat. Photonics **4**, 655–660 (2010).
12. M. Avenhaus, K. Laiho, M. V. Chekhova, and C. Silberhorn, "Accessing higher order correlations in quantum optical states by time multiplexing," Phys. Rev. Lett. **104**, 063602 (2010).
13. R. Nehra, A. Win, M. Eaton, R. Shahrokhshahi, N. Sridhar, T. Gerrits, A. Lita, S. W. Nam, and O. Pfister, "State-independent quantum state tomography by photon-number-resolving measurements," Optica **6**, 1356–1360 (2019).
14. L. Cohen, E. S. Matekole, Y. Sher, D. Istrati, H. S. Eisenberg, and J. P. Dowling, "Thresholded quantum LIDAR: exploiting photon-number-resolving detection," Phys. Rev. Lett. **123**, 203601 (2019).
15. F. E. Becerra, J. Fan, and A. Migdall, "Photon number resolution enables quantum receiver for realistic coherent optical communications," Nat. Photonics **9**, 48–53 (2015).
16. Y.-H. Zhou, Z.-W. Yu, and X.-B. Wang, "Making the decoy-state measurement-device-independent quantum key distribution practically useful," Phys. Rev. A **93**, 042324 (2016).
17. H.-L. Yin, T.-Y. Chen, Z.-W. Yu, H. Liu, L.-X. You, Y.-H. Zhou, S.-J. Chen, Y. Mao, M.-Q. Huang, W.-J. Zhang, H. Chen, M. J. Li, D. Nolan, F. Zhou, X. Jiang, Z. Wang, Q. Zhang, X.-B. Wang, and J.-W. Pan, "Measurement-device-independent quantum key distribution over a 404 km optical fiber," Phys. Rev. Lett. **117**, 190501 (2016).
18. G. Temporão, S. Tanzilli, H. Zbinden, N. Gisin, T. Aellen, M. Giovannini, and J. Faist, "Mid-infrared single-photon counting," Opt. Lett. **31**, 1094–1096 (2006).
19. Q. Zhou, K. Huang, H. Pan, E. Wu, and H. Zeng, "Ultrasensitive mid-infrared up-conversion imaging at few-photon level," Appl. Phys. Lett. **102**, 241110 (2013).
20. M. Mancinelli, A. Trenti, S. Piccione, G. Fontana, J. S. Dam, P. Tidemand-Lichtenberg, C. Pedersen, and L. Pavesi, "Mid-infrared coincidence measurements on twin photons at room temperature," Nat. Commun. **8**, 15184 (2017).
21. M. Mrejen, Y. Erlich, A. Levanon, and H. Suchowski, "Multicolor time-resolved upconversion imaging by adiabatic sum frequency conversion," Laser Photon. Rev. **14**, 2000040 (2020).
22. T. W. Neely, L. Nugent-Glandorf, F. Adler, and S. A. Diddams, "Broadband mid-infrared frequency upconversion and spectroscopy with an aperiodically poled $LiNbO_3$ waveguide," Opt. Lett. **37**, 4332–4334 (2012).
23. L. Lehmann, L. Grossard, L. Delage, F. Reynaud, M. Chauvet, and F. Bassignot, "Single photon MIR upconversion detector at room

temperature with a PPLN ridge waveguide," Opt. Express **27**, 19233–19241 (2019).
24. X. Liu, B. Kuyken, G. Roelkens, R. Baets, R. M. Osgood, and W. M. J. Green, "Bridging the mid-infrared-to-telecom gap with silicon nanophotonic spectral translation," Nat. Photonics **6**, 667–671 (2012).
25. Q. Zheng, H. Zhu, S.-C. Chen, C. Tang, E. Ma, and X. Chen, "Frequency-upconverted stimulated emission by simultaneous five-photon absorption," Nat. Photonics **7**, 234–239 (2013).
26. D. A. Fishman, C. M. Cirloganu, S. Webster, L. A. Padilha, M. Monroe, D. J. Hagan, and E. W. V. Stryland, "Sensitive mid-infrared detection in wide-bandgap semiconductors using extreme non-degenerate two-photon absorption," Nat. Photonics **5**, 561–565 (2011).
27. J. S. Dam, P. Tidemand-Lichtenberg, and C. Pedersen, "Room-temperature mid-infrared single-photon spectral imaging," Nat. Photonics **6**, 788–793 (2012).
28. D. Knez, A. M. Hanninen, R. C. Prince, E. O. Potma, and D. A. Fishman, "Infrared chemical imaging through non-degenerate two-photon absorption in silicon-based cameras," Light Sci. Appl. **9**, 125 (2020).
29. R. Demur, A. Grisard, L. Morvan, E. Lallier, N. Treps, and C. Fabre, "High sensitivity narrowband wavelength mid-infrared detection at room temperature," Opt. Lett. **42**, 2006–2009 (2017).
30. J. S. Pelc, L. Ma, C. R. Phillips, Q. Zhang, C. Langrock, O. Slattery, X. Tang, and M. M. Fejer, "Long-wavelength-pumped upconversion single-photon detector at 1550 nm: performance and noise analysis," Opt. Express **19**, 21445–21456 (2011).
31. K. Huang, X. Gu, H. Pan, E. Wu, and H. Zeng, "Few-photon-level two-dimensional infrared imaging by coincidence frequency upconversion," Appl. Phys. Lett. **100**, 151102 (2012).
32. K. Huang, X. R. Gu, H. F. Pan, E. Wu, and H. P. Zeng, "Synchronized fiber lasers for efficient coincidence single-photon frequency upconversion," IEEE J. Sel. Top. Quantum Electron. **18**, 562–566 (2012).
33. T. Xiang, Q.-C. Sun, Y. Li, Y. Zheng, and X. Chen, "Single-photon frequency conversion via cascaded quadratic nonlinear processes," Phys. Rev. A **97**, 063810 (2018).
34. R. L. Pedersen, L. Høgstedt, A. Barh, L. Meng, and P. Tidemand-Lichtenberg, "Characterization of the NEP of mid-infrared upconversion detectors," IEEE Photon. Technol. Lett. **31**, 681–684 (2019).
35. E. Pomarico, B. Sanguinetti, R. Thew, and H. Zbinden, "Room temperature photon number resolving detector for infared wavelengths," Opt. Express **18**, 10750–10759 (2010).
36. K. Huang, X. Gu, M. Ren, Y. Jian, H. Pan, G. Wu, E. Wu, and H. Zeng, "Photon-number-resolving detection at 1040 μm coincidence frequency upconversion," Opt. Lett. **36**, 1722–1724 (2011).
37. R. A. McCracken, F. Graffitti, and A. Fedrizzi, "Numerical investigation of mid-infrared single-photon generation," J. Opt. Soc. Am. B **35**, C38–C48 (2018).
38. Y. M. Sua, H. Fan, A. Shahverdi, J.-Y. Chen, and Y.-P. Huang, "Direct generation and detection of quantum correlated photons with 3.2 μm wavelength spacing," Sci. Rep. **7**, 17494 (2017).
39. S. Tanzilli, W. Tittel, M. Halder, O. Alibart, P. Baldi, N. Gisin, and H. Zbinden, "A photonic quantum information interface," Nature **437**, 116–120 (2005).
40. H. Takesue, "Single-photon frequency down-conversion experiment," Phys. Rev. A **82**, 013833 (2010).
41. K. Huang, X. Gu, Q. Zhou, H. Pan, E. Wu, and H. Zeng, "Efficient generation of mid-infrared photons at 3.16 μm by coincidence frequency downconversion," Laser Phys. **23**, 045401 (2013).
42. J. Zeng, B. Li, Q. Hao, M. Yan, K. Huang, and H. Zeng, "Passively synchronized dual-color mode-locked fiber lasers based on nonlinear amplifying loop mirrors," Opt. Lett. **44**, 5061–5064 (2019).
43. W. Kang, B. Li, Y. Liang, Q. Hao, M. Yan, K. Huang, and H. Zeng, "Coincidence-pumping upconversion detector based on passively synchronized fiber laser system," IEEE Photon. Technol. Lett. **32**, 184–187 (2020).
44. L. Meng, L. Høgstedt, P. Tidemand-Lichtenberg, C. Pedersen, and P. John Rodrigo, "Enhancing the detectivity of an upconversion single-photon detector by spatial filtering of upconverted parametric fluorescence," Opt. Express **26**, 24712–24722 (2018).
45. M. Widarsson, M. Henriksson, P. Mutter, C. Canalias, V. Pasiskevicius, and F. Laurell, "High resolution and sensitivity upconversion mid-infrared photon-counting LIDAR," Appl. Opt. **59**, 2365–2369 (2020).
46. S. Wolf, T. Trendle, J. Kiessling, J. Herbst, K. Buse, and F. Kühnemann, "Self-gated mid-infrared short pulse upconversion detection for gas sensing," Opt. Express **25**, 24459–24468 (2017).
47. Z. Bao, Y. Liang, Z. Wang, Z. Li, E. Wu, G. Wu, and H. Zeng, "Laser ranging at few-photon level by photon-number-resolving detection," Appl. Opt. **53**, 3908–3912 (2014).
48. C.-Q. Hu, Z.-Q. Yan, J. Gao, Z.-Q. Jiao, Z.-M. Li, W.-G. Shen, Y. Chen, R.-J. Ren, L.-F. Qiao, A.-L. Yang, H. Tang, and X.-M. Jin, "Transmission of photonic polarization states through 55-m water: towards air-to-sea quantum communication," Photon. Res. **7**, A40–A44 (2019).